

Application of Lateral Boundary Condition Perturbations to Help Restore Dispersion in Limited-Area Ensemble Forecasts

PAUL NUTTER* AND MING XUE

School of Meteorology, and Center for Analysis and Prediction of Storms, University of Oklahoma, Norman, Oklahoma

DAVID STENSRUD

National Severe Storms Laboratory, Norman, Oklahoma

(Manuscript received 15 September 2003, in final form 3 March 2004)

ABSTRACT

In a companion paper, the authors showed that lateral boundary condition (LBC) constraints on small-scale error variance growth are sufficient to limit dispersion in limited-area-model (LAM) ensemble simulations. The error growth constraints result from the use of coarsely resolved and temporally interpolated LBCs. The effect is present in any modeling system using “one-way” LBC forcing unless the forcing model has the same resolution as the LAM and the LBCs are updated at every time step. This limitation suggests the need to apply statistically consistent, finescale LBC perturbations at every time step during LAM simulations. In this paper, a new method for implementing LBC perturbations is developed to help counter the above effect by creating a statistically consistent source of error growth along the lateral boundaries. The LBC perturbations are designed to amplify with time while coherently propagating into the domain.

The procedure is tested in a controlled and efficient manner using a modified barotropic channel model. Ten-member ensemble simulations are produced over many cases on a periodic channel domain and each of four smaller nested domains. Lateral boundary effects are specifically isolated since the simulations are perfect except for initial and lateral boundary condition perturbations and the use of coarsely resolved and/or temporally interpolated one-way LBCs. Statistical results accumulated over 100 independent cases demonstrate that the application of LBC perturbations capably restores ensemble dispersion, especially on smaller domains where LBC effects propagate quickly through the domain. The paper closes with some comments on the relevance of the LBC perturbation procedure in practical settings.

1. Introduction

In a companion paper, Nutter et al. (2004) showed that the use of coarsely resolved and/or temporally interpolated lateral boundary conditions (LBCs) is sufficient to cause underdispersive limited-area-model (LAM) ensemble forecasts. Although this result was measured using a simplified model configuration, the effect is present to some extent in all typical modeling systems using “one-way” LBC forcing. In practice, these LBC constraints can be minimized by operating very large regional domains, or they can simply be ignored at the discretion of the model’s developer. The LBC constraints may have great significance for LAM configurations having relatively smaller regional do-

main, especially those used by smaller groups for ensemble forecasting or storm-scale predictions. Hence, in this paper we explore the possibility that LBC constraints on error variance growth and ensemble spread may be avoided by applying statistically consistent, fine-scale LBC perturbations at every time step throughout the LAM simulations.

The use of coarsely resolved and temporally interpolated LBCs restricts small-scale error growth in LAMs because of the LBC “sweeping” effects that were documented by Nutter et al. (2004) using a carefully controlled approach. This limitation of LAMs has important consequences because it artificially inflates estimates of predictability limits which, in turn, erroneously decreases the apparent forecast uncertainty. The LBC sweeping mechanism associated with coarsely resolved LBCs has been considered previously by a number of authors including Errico and Baumhefner (1987), Vukicevic and Errico (1990), Paegle et al. (1997), Warner et al. (1997), Hou et al. (2001), and De Elía and Laprise (2002). Nutter et al. (2004) additionally considered error growth constraints introduced by temporal

* Current affiliation: Cooperative Institute for Mesoscale Meteorological Studies, University of Oklahoma, Norman, Oklahoma.

Corresponding author address: Dr. Paul Nutter, CIMMS, University of Oklahoma, 100 E. Boyd St., Rm. 1110, Norman, OK 73019.
E-mail: pnutter@ou.edu

interpolation between relatively infrequent LBC updates and extended the analysis to quantify the impact on LAM ensemble dispersion. In combination, these LBC constraints are present in any LAM using one-way LBC forcing and are sufficient to contribute to the reduction of LAM ensemble dispersion.

To help improve the design of LAM ensemble systems, LBC perturbations are introduced in this paper to offset LBC sweeping effects by creating a statistically consistent source of error growth along the lateral boundaries. The LBC perturbations are designed to amplify with time while coherently propagating into the domain. The perturbations are shown to help restore small-scale error growth that would otherwise be swept away through the downstream boundary.

The application of LBC perturbations described herein has not previously been attempted to the authors' knowledge. The method goes beyond the common (and essential) practice of using an ensemble of unique LBCs provided by individual members of an external model ensemble. Earlier results by Nutter et al. (2004) showed that an ensemble of LBCs does not mitigate the LBC constraint on error growth at small scales because the LBCs are still coarsely resolved in both space and time. Hence, the LBC perturbation method described here is superposed upon the full set of LBCs originating as output from an ensemble of external model forecasts.¹

We begin in section 2 with a brief review of the simplified model configuration and statistical measures that were used by Nutter et al. (2004). A detailed description of the LBC perturbation procedure is given in section 3. Statistical results shown in section 4 quantify how well the perturbations help restore LAM ensemble dispersion. Concluding remarks address the need for additional development before LBC perturbations can be applied in operational settings.

2. Configuration of numerical experiments

a. Numerical model and its configurations

Numerical experiments for this work are conducted using the same single-level modified barotropic vorticity channel model used by Nutter et al. (2004). The model is configured specifically to isolate the effects of LBCs on LAM ensemble dispersion while avoiding analysis and model system errors. Although simplified, the model remains nonlinear, dispersive, and sensitive to initial condition (IC) perturbations. The model is based on a parameterized version of the quasigeostrophic potential

vorticity equation (Holton 1979, section 8.4.2), so we call it the parameterized potential vorticity (PPV) model. The model and its numerics are described fully in Nutter (2003) and summarized in Nutter et al. (2004).

PPV model simulations are run with "global" and limited-domain configurations. Both configurations operate with the same time step and with 25-km grid spacing to avoid the impact of numerical discretization errors when comparing simulations to a model-generated truth. The global model configuration is a zonally periodic channel domain dimensioned 18 000 km from west to east and 6000 km from south to north. Four different LAM domains are defined as subsets of the periodic channel domain (see Fig. 1 in Nutter et al. 2004). The largest nested domain is (6000 km)², the medium-sized domain is (3000 km)², and the two smallest domains are (1500 km)². One of the small domains is displaced southward in the channel relative to the centralized position of the others to evaluate error growth in a less unstable part of the flow.

The LAM simulations are configured using one-way Dirichlet boundary conditions for streamfunction (ψ) and parameterized potential vorticity (ξ) obtained from subsets of the global model simulations. The one-way LBC scheme used in the LAM simulations applies a seven-point peripheral relaxation zone (Davies 1976, 1983) for ξ . Boundary values of ψ are then specified before obtaining ψ across the limited domain by inverting a Helmholtz equation for ξ (Nutter et al. 2004). Simpler methods may be used for applying LBCs in a quasigeostrophic model (Charney et al. 1950), but we use the one-way scheme because it is currently used in most configurations of atmospheric LAMs.

LBCs are obtained by linearly interpolating between subsets of the global simulations at 1-, 3-, and 6-hourly intervals. Coarsely resolved LBC fields are generated by applying a low-pass spatial filter to fields from global model simulations running at the same resolution as the LAM. The low-pass filter is a Fourier transform procedure (Errico 1985; Laprise et al. 2000; Nutter 2003) that removes completely all wavelengths shorter than 150 km while perfectly retaining the amplitudes of wavelengths longer than 450 km. The filtering process preserves the accuracy of large-scale motions while removing those which would not be present on a grid having 3 times less spatial resolution as the LAM grid. This analysis procedure is similar to that used most recently by Laprise et al. (2000) and De Elía and Laprise (2002).

One hundred independent 10-member ensemble simulations are constructed by assigning perturbations to initial conditions given random states from the model-generated climatology (Nutter 2003; Nutter et al. 2004).

b. Ensemble statistics

Given a forecast ensemble \mathbf{f}_i , $i = 1 \dots N$, and the verifying analysis \mathbf{a} , Nutter et al. (2004) showed that

¹ The set of "perturbed" LBCs traditionally refers to the set of unique LBCs provided by an external model ensemble. The reader should be aware that this terminology is somewhat misleading for the set of external LBCs because perturbations are applied only to their initial states, which are then allowed to grow freely without further intervention. In contrast, the LBC perturbations described herein are applied to the existing set of external LBCs throughout the LAM simulation.

we can link ensemble dispersion to the spectral decomposition of total error variance using the relation

$$D^2 = \sigma^2 + \frac{1}{N} \sum_{i=1}^N (\langle \mathbf{f}_i \rangle - \langle \mathbf{a} \rangle)^2 - \|\bar{\mathbf{f}} - \mathbf{a}\|^2, \quad (1)$$

where $\langle \cdot \rangle$ denotes a spatial average and $\|\cdot\|^2$ is the average sum of squares (dot product) over the grid. The ensemble dispersion (D^2) is the square of the ensemble spread (deviation about its mean), and σ^2 is the ensemble's total biased error variance. The remaining terms are, respectively, the ensemble mean square spatial error (sme)² and the squared error of the ensemble mean (eme)².

Equation (1) will be applied in section 4 to evaluate the extent to which perturbed LBCs help restore ensemble dispersion. Toward this end, the total biased error variance (σ^2) may be obtained spectrally as (Errico 1985)

$$\sigma^2 = \frac{1}{N} \sum_{i=1}^N \sum_{\kappa=1}^{K-1} 2|F_i(\kappa)|^2, \quad (2)$$

where $F_i(\kappa)$ is the discrete Fourier transform of $\mathbf{f}_i - \mathbf{a}$ and $\kappa = 1, \dots, K - 1$ are the set of Nyquist resolved wavenumbers on the grid (Errico 1985). When σ^2 is obtained spectrally for limited-area domains, the result is slightly greater than the spatially integrated error variance because detrending the fields before the transform introduces variance at small scales (Errico 1985). However, the spectral variance inflation is present for all model configurations tested in this work, so it does not invalidate the intercomparison of results obtained using different LBC treatments.

The latter two terms in (1) cannot be decomposed in a simple way to reveal their contributions to D^2 at different scales. However, if these terms are nearly the same for both global and LAM simulations, then their contributions to D^2 are negated under comparison. Under this condition, the spectral relation between error variance and ensemble dispersion is maintained. In the perfect model simulations conducted for this work, the ensembles are unbiased and the spatial error term is negligible on large domains. However, on small domains, the spectral calculation of ensemble dispersion could become distorted because of phase errors introduced by upscale perturbation growth. The ensemble bias term could become large in practical application because of model deficiencies. However, ensembles can be calibrated to remove such biases (Hamill and Colucci 1997; Hamill 2001).

All diagnostics for this work are presented in terms of vorticity because it retains more power in the PPV model at small scales than do the streamfunction, velocity, or kinetic energy (Nutter 2003).

3. LBC perturbations

The procedures used to develop and apply LBC perturbations to the LAM ensemble simulations are detailed

in this section. The general procedure for implementing LBC perturbations at each time step is as follows (details to follow). A two-dimensional perturbation field is generated on the LAM grid using inverse Fourier transforms. The perturbation field has zero mean and is periodic in both x and y directions. The LBC perturbation field is initialized by assigning random phase angles to each wavenumber. Amplitudes of the perturbations are determined by the loss of error variance at specific wavelengths due to LBC effects. Once initialized, the field is translated at the Rossby phase speed for each wavenumber so that perturbations passing through the lateral boundary remain coherent in both space and time. Perturbation amplitudes increase with time based on the amount of error variance needed to restore the portion lost due to LBC sweeping. After the perturbation field is constructed, it is added to the spatially and temporally interpolated LBC field given by subsets of an external model simulation. The perturbed LBC field is then blended with the LAM solution only within a peripheral wave relaxation zone at each time step.

a. Implementation

1) PHASE ANGLE FORM OF FOURIER SERIES

The net effect of using coarsely resolved and temporally interpolated LBCs is a loss of variance at small scales, and hence, a reduction in the total biased error variance (Nutter et al. 2004). The total biased error variance [Eq. (2)] is computed using one-dimensional spectra as described in section 2. The error variance calculations retain only wave amplitudes for isotropic wavenumbers and are averaged over many independent cases. The phase angle form of the Fourier series (e.g., Walker 1988) is most compatible with this statistical framework and is used to synthesize random fields having predetermined error variance spectra.

Consider the Fourier series expansion of a one-dimensional periodic function $f(x) = f(x + L)$:

$$f(x) = a_0 + \sum_{k=1}^{\infty} \left[a_k \cos\left(\frac{2\pi kx}{L}\right) + b_k \sin\left(\frac{2\pi kx}{L}\right) \right], \quad (3)$$

where a_k and b_k are real amplitude coefficients. The phase-angle form of the Fourier series is obtained by letting $a_k = c_k \cos(-\theta_k)$ and $b_k = c_k \sin(-\theta_k)$, where $c_k = \sqrt{a_k^2 + b_k^2}$ and θ_k is the phase angle for wavenumber k . Apply these definitions for a_k and b_k in (3) and manipulate so that

$$\begin{aligned} f(x) &= a_0 + \sum_{k=1}^{\infty} \left[c_k \cos(\theta_k) \cos\left(\frac{2\pi kx}{L}\right) \right. \\ &\quad \left. - c_k \sin(\theta_k) \sin\left(\frac{2\pi kx}{L}\right) \right] \\ &= a_0 + \sum_{k=1}^{\infty} \left[c_k \cos\left(\frac{2\pi kx}{L} + \theta_k\right) \right] \end{aligned}$$

$$= a_0 + \frac{1}{2} \sum_{k=1}^{\infty} [c_k e^{i\theta_k} e^{i(2\pi kx/L)} + c_k e^{-i\theta_k} e^{-i(2\pi kx/L)}]. \quad (4)$$

Equation (4) shows that a periodic function can be synthesized simply by specifying a real amplitude coefficient (c_k) and phase angle (θ_k) for each wavenumber k . This form is useful because the one-dimensional variance spectra retain only the magnitudes of complex Fourier coefficients. The phase angles remain unknown but may be specified randomly.

Fast Fourier transform (FFT) algorithms use the complex form of the Fourier series. To convert (4) to the more useful complex form, introduce complex Fourier coefficients

$$\begin{aligned} F(0) &= a_0, & F(k) &= \frac{1}{2} c_k e^{i\theta_k} = \frac{1}{2} (a_k - ib_k), \\ F(-k) &= \frac{1}{2} c_k e^{-i\theta_k} = \frac{1}{2} (a_k + ib_k). \end{aligned} \quad (5)$$

Apply these coefficients in (4) so that

$$\begin{aligned} f(x) &= F(0) + \sum_{k=1}^{\infty} [F(k) e^{2\pi i k x / L} + F(-k) e^{-2\pi i k x / L}] \\ &= \sum_{k=0}^{\infty} F(k) e^{2\pi i k x / L} + \sum_{k=-1}^{-\infty} F(k) e^{2\pi i k x / L} \\ &= \sum_{k=-\infty}^{\infty} F(k) e^{2\pi i k x / L}. \end{aligned} \quad (6)$$

The extension of Eqs. (3) to (6) into their two-dimensional forms is not difficult but involves many additional terms. While details of the derivation are omitted (see Walker 1988), the complex form of the Fourier series for a two-dimensional periodic field $f(x, y) = f(x + L_x + L_y)$ is

$$f(x, y) = \sum_{k=-\infty}^{\infty} \sum_{l=-\infty}^{\infty} F(k, l) \exp \left[2\pi i \left(\frac{kx}{L_x} + \frac{ly}{L_y} \right) \right]. \quad (7)$$

The discrete Fourier series used for the calculations is

$$f(x, y) \approx \sum_{k=-N_x/2+1}^{N_x/2} \sum_{l=-N_y/2+1}^{N_y/2} F(k, l) \exp \left[2\pi i \left(\frac{kx}{L_x} + \frac{ly}{L_y} \right) \right], \quad (8)$$

where $x = (k + N_x/2 + 1)\Delta x$ and $y = (l + N_y/2 + 1)\Delta y$. Even integers N_x and N_y denote the number of grid points along each dimension of the domain. In practice, Fourier series approximation of real fields makes use of complex conjugate symmetries so that the negative l wavenumbers are omitted (Press et al. 1992).

Equation (8) can be used to synthesize a field having predetermined variance spectra $|F'(k, l)|^2$ and random phase angles $\theta_{k,l}$ by specifying

$$F(k, l) = \sqrt{\frac{|F'(k, l)|^2}{2}} (\cos\theta_{k,l} + i \sin\theta_{k,l}), \quad (9)$$

except the factor of 1/2 is omitted for $k = 0$ and $k = N_x/2$. This factor is required since error variance spectra obtained previously using FFT algorithms were multiplied by 2 because of the complex conjugate symmetry in transforms of real data.

2) AMPLITUDE OF PERTURBATIONS

Amplitudes of the LBC perturbations are defined by the predetermined loss of error variance at specific wavelengths due to LBC effects (Nutter et al. 2004). Thus, if σ_{κ}^2 denotes the one-dimensional error variance spectra obtained from previous global and LAM simulations, amplitudes of the perturbation spectra are determined using (9) with

$$|F'(k, l)|^2 = \sigma_{\kappa}^2(\text{global}) - \sigma_{\kappa}^2(\text{LAM}), \quad (10)$$

where $\kappa = \sqrt{k^2 + l^2}$. The perturbation spectra are distributed equally among all the wavenumber pairs (k, l) contained within each annular wavenumber ring $\mathfrak{K}(\kappa) \pm (1/2)\delta\kappa$, where \mathfrak{K} denotes nearest integer. Variances are set to zero for wavenumber pairs where κ exceeds that of the smallest resolved wavelength since these were not accumulated in the one-dimensional spectra. Furthermore, negative values of $|F'(k, l)|^2$ are set to zero because, in this case, the error variance in the LAM simulations already exceeds that of the global simulations.

Results in Fig. 1 show $|F'(k, l)|^2$ obtained for the LAM ensemble configuration having 3-hourly updated, low-pass-filtered LBCs. Difference spectra are negative for about the first 12 h, indicating that the LAM simulations have more error variance than do the corresponding subsets of the global simulations. The additional error is introduced almost immediately when the Helmholtz equation is solved to obtain streamfunction from smoothed LBCs (Nutter et al. 2004, section 5). Errors are created at first along the boundaries, but then pass through the domain so that further growth becomes limited by the LBC constraints discussed in detail by Nutter et al. (2004). After about 12–18 h, laterally unconstrained error variance growth in the global simulations exceeds that measured in the LAM simulations.

When the difference spectra are negative, amplitudes of the LBC perturbation field are set to zero, depending on wavelength. At later times, the amplitude of the perturbation is greatest at wavelengths between about 100 and 1000 km. Indeed, these are the scales that were most strongly affected by the filtering effects associated with spatial and temporal filtering of LBCs (Nutter et al. 2004). Difference spectra are not shown beyond 72 h because there is minimal additional growth beyond this time. Hence, the LBC perturbation field constructed using the difference spectra in Fig. 1 begin with zero amplitude, then begin to grow after about 12 h until reaching a nearly constant value around 72 h.

The difference spectra for these simulations were computed each hour. These spectra were interpolated

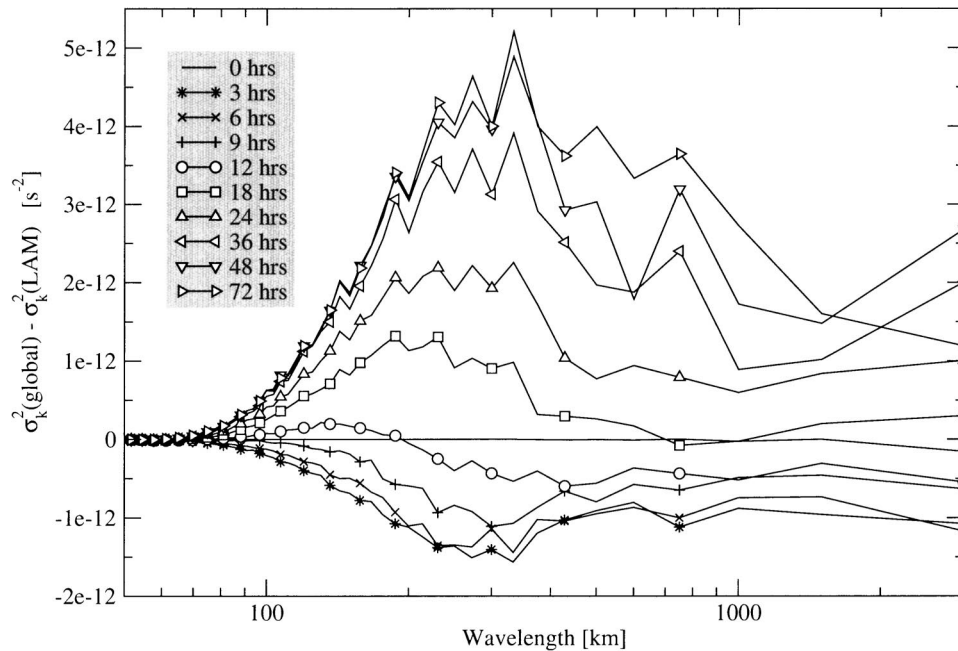


FIG. 1. Difference in error variance spectra ($\times 10^{-12} \text{ s}^{-2}$) between global ensemble simulations and LAM ensemble simulations having 3-hourly updated, low-pass-filtered LBCs.

linearly in time before generating LBC perturbation fields at every 7.5-min time step of the PPV model. Temporal interpolation of the spectra before generating the perturbation field does not reduce small-scale variance as does interpolation between external LBC fields. Furthermore, temporal changes in the difference spectra are small since statistics were obtained as averages over 100 cases. In practical applications, data will not be available hourly, perhaps only every 3, or 6, h. A possible approach for these scenarios is to fit analytic curves to the set of difference spectra (e.g., Lorenz 1982; Dalcher and Kalnay 1987; Schubert and Suarez 1989; Stroe and Royer 1993; Reynolds et al. 1994; De Elía and Laprise 2002). Attempts were made to fit such curves here, but it was difficult to obtain parameters that produced accurate fits across all scales of motion. This is an issue that should be addressed further with application to more complex atmospheric LAMs.

3) TRANSLATING THE PERTURBATION FIELD

The perturbation field is initialized by specifying uniform random phase angles $0 \leq \theta_{k,l} \leq 2\pi$ in (9). Once initialized, the phase angles are stored and incremented at each time step to cause a translation of the perturbation field when it is synthesized using (8). This translation is important for providing temporally and spatially coherent wave structures as they pass through the lateral boundary. The field is translated at some characteristic speed c_κ by incrementing the phase angles such that

$$\theta_{k,l}(t + \Delta t) = \theta_{k,l}(t) + \kappa c_\kappa \Delta t, \quad (11)$$

where again, $\kappa = \sqrt{k^2 + l^2}$.

An appropriate choice of translation speed for this work is the Rossby phase speed. Since the available error variance spectra are one-dimensional, we use the isotropic, or unidirectional phase speed

$$c_\kappa = (U_0 k - \beta k / \kappa^2) / \kappa, \quad (12)$$

where U_0 is the base-state zonal flow speed.

Rossby phase speeds calculated using specified PPV model constants are less than 12 m s^{-1} . The x component of group velocity remains near 12 m s^{-1} while the y component of group velocity is generally less than 0.001 m s^{-1} . Thus, the entire perturbation field translates from west to east at about 12 m s^{-1} . This propagation speed implies that the perturbation field will affect the breadth of the small, medium, and large limited-area domains in about 35, 70, and 140 h, respectively. However, examination of many individual simulations (Nutter 2003) reveals that LBC errors completely infect these respective subdomains in about 24, 36, and 60 h when using 3-hourly LBC updates, and progress about 25% faster when using 6-hourly updates. The more rapid rate of error propagation is due to the superposition of the zonal jet on the base-state flow, and also because the Helmholtz equation is inverted to obtain streamfunction with LBC interpolation errors occurring at increasingly larger scales. It is clear from these arguments that the specified speed of the LBC perturbation field is somewhat conservative, although supported by dynamical equations of motion. Other choices for the translation speed could

be more appropriate in applications using full primitive equation models. This question remains beyond the scope of the present study.

b. Example simulation with perturbed LBCs

An example perturbation vorticity field (ζ') was constructed at multiple times using (8) with the difference spectra in Fig. 1. Results are shown in Fig. 2. Streamfunction perturbations are obtained by solving the Poisson equation $\nabla^2\psi' = \zeta'$. The solution to the Poisson equation is unique to within a constant value when using periodic boundary conditions. Therefore, the spatial mean $\langle\psi'\rangle$ was subtracted from each solution to ensure that the perturbation streamfunction remains unbiased.

As explained previously, error variances from the LAM simulation are greater than those of the global simulations for about the first 12 h. Therefore, the amplitude of vorticity perturbations are set to zero since the LAM simulation already has excessive error variance during this time. The impact of this choice is seen in Figs. 2a and 2b as the perturbation field does not begin to amplify until about 15 h have passed. Careful examination of the vorticity perturbation field reveals about 10 to 20 wave couplets across the breadth of the $(3000\text{-km})^2$ domain. This result is consistent with the difference spectra shown in Fig. 1 since wavelengths are on the order of 150 to 300 km.

The vorticity field is translated at the Rossby phase velocity using (11) and (12). Motion from west to east is clearly evident in time animation of these fields and is also seen in Fig. 2 by locating and tracking local minima and maxima. The translation and simultaneous amplification of the perturbation field is more easily seen in the streamfunction perturbations. Using the approximation $\Phi' = \psi'f$, note that the contours of ψ' correspond to $10\text{ m}^2\text{ s}^{-2}$ increments of geopotential height.

The vorticity and streamfunction perturbations fields are constructed at each time step, and at the spatial resolution of a LAM simulation. The perturbations are then added to the temporally interpolated LBC field provided by a coarsely resolved external model simulation. This perturbed external LBC field is then blended with the LAM solution across the peripheral 7-point relaxation zone. The perturbations are produced as a field covering the entire LAM domain to ensure that the spatial variance is restored using coherent wave patterns. However, *the perturbations are applied only within the boundary zone and modify the LAM solution only after propagating into the domain.*

An example LAM ensemble obtained from simulations having perturbed LBCs is shown in Fig. 3 with its dispersion loss ratio [Eq. (15) in Nutter et al. 2004]. At locations where the loss ratio is negative, the LAM ensemble has less dispersion than the global ensemble. The “spaghetti” contours and streamfunction dispersion (represented by the solid and dashed lines) appear much

the same as in Fig. 12 of Nutter et al. (2004). Hence, the LBC perturbations have not ruined the individual ensemble member simulations by introducing excessive noise.

The effects of the LBC perturbations for this example are seen in the dispersion loss ratio, when compared to the unperturbed simulation shown as Fig. 12 in Nutter et al. (2004). During the first 12 to 24 h, the dispersion loss ratio is similar in both perturbed and unperturbed simulations. This is expected since the amplitude of the perturbations is zero through the first 12 h, as discussed previously. Once the LBC perturbations begin to enter the LAM domain, they help enhance error variance locally and the dispersion loss ratio becomes less negative compared to the unperturbed simulation. Comparison of the simulations after about 60 h shows that LBC perturbations have swept through the domain. Specifically, regions of increased and decreased vorticity dispersion relative to the global simulation now appear evenly distributed throughout the domain. The LBC perturbations do not apply instantaneously across the breadth of the domain, but instead propagate inward to restore those scales that have been filtered out by LBC filtering and sweeping effects. After 96 h, the domain average dispersion loss ratio is -0.95 for the unperturbed simulation and -0.11 for the perturbed simulation. Hence, the impact of the LBC perturbations has been to restore LAM ensemble dispersion from a loss of nearly 50% to a loss of just 10% relative to the global ensemble simulations.

4. Statistical results

The LAM ensemble simulations run by Nutter et al. (2004) are repeated here, except LBC perturbations are created and applied at each time step during the simulations as discussed in the previous section. Statistical results are obtained as averages over 100 independent 10-member LAM ensemble simulations and are compared to results obtained from the earlier unperturbed LAM simulations and also to those obtained from subsets of global model simulations.

a. Ensemble error variance spectra

Consider results from the LAM ensemble configuration having 3-hourly updated, low-pass-filtered (coarsely resolved) LBCs that are perturbed at every time step (Fig. 4). Normalized error variances [see Eq. (12) in Nutter et al. 2004] reveal that the application of LBC perturbations completely restores error variances at wavelengths longer than about 500 km to values obtained from the control simulations run on the global domain. The LBC perturbations are less effective for smaller scales, where the proportion of error variance restored depends on domain size. For example, on the large domain (Fig. 4a), the LBC perturbations restore about 1/3 of the error variance lost at saturation in the

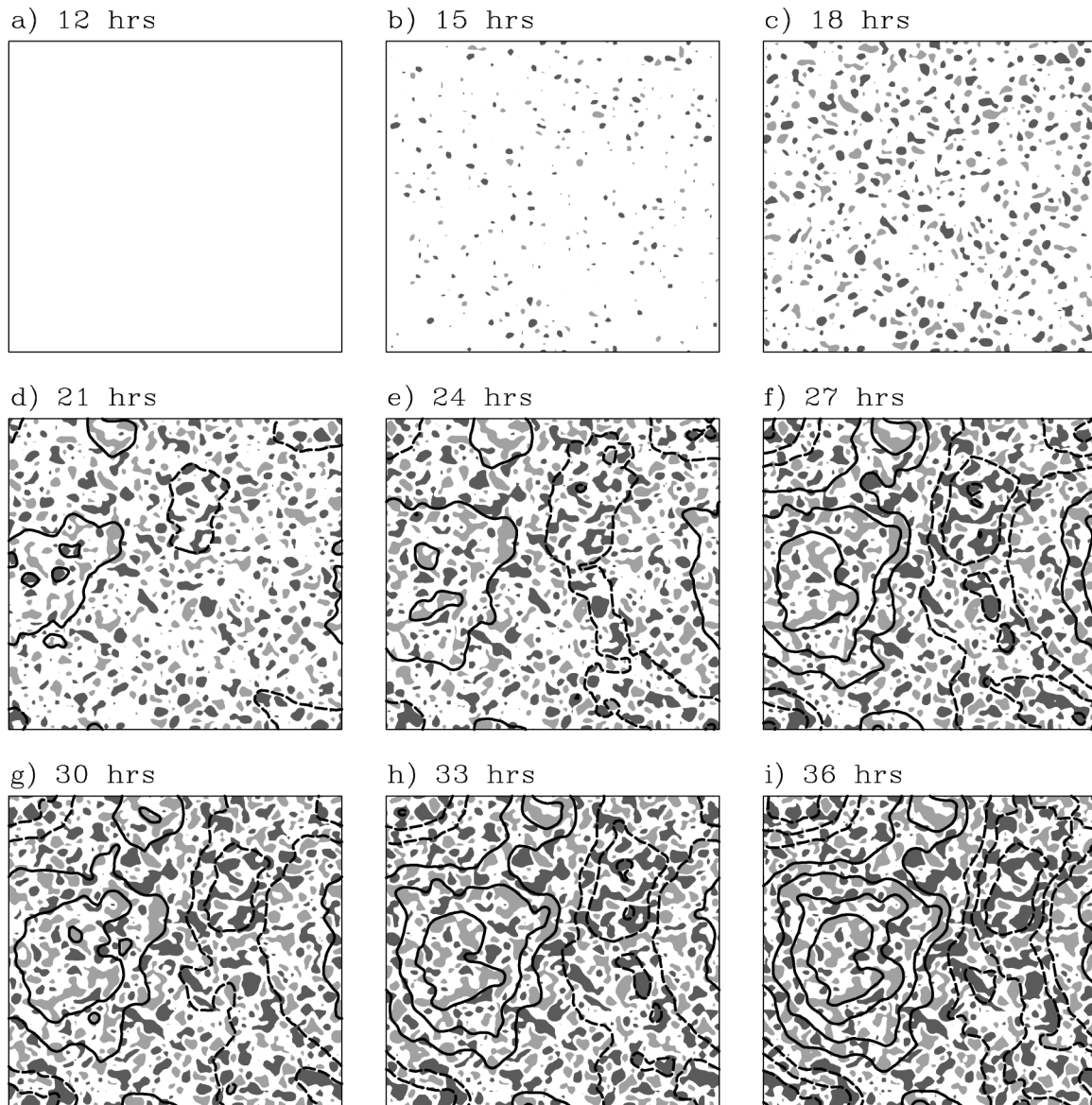


FIG. 2. Example of LBC perturbation fields constructed for the medium domain using the difference in error variance spectra between global ensembles and LAM ensembles having 3-hourly updated, low-pass-filtered LBCs (Fig. 1). Positive (negative) vorticity perturbations exceeding $0.5 \times 10^{-5} \text{ s}^{-1}$ are indicated by light (dark) shades. Positive (negative) streamfunction perturbations are shown with solid (dashed) contours at $\pm 0.1 \times 10^6 \text{ m}^2 \text{ s}^{-1}$ intervals (zero line omitted).

smallest scales. Compare this to the small, centered domain (Fig. 4c), where the LBC perturbations restore more than 3/4 of the error variance lost in the unperturbed LAM simulations.

To explain these results, note that difference spectra used to determine the amplitude of LBC perturbations [Eq. (10)] are based on error variance calculations obtained from data over the full extent of the LAM domain. However, LBC perturbations are applied only within the peripheral 7-point wave-absorbing zone. The perturbations subsequently disperse and/or dissipate while propagating through the LAM domain. Furthermore, as noted previously, the phase propagation speed of the

perturbation field is a conservative estimate of the rate at which errors pass through the domain. For these reasons, the difference spectra likely underestimate the amplitude of LBC perturbations needed to fully restore LAM error variances to those obtained from global simulations. The LBC perturbations are more effective on smaller domains because there is less time for dispersion and dissipation to reduce their impact while passing through the LAM domain.

There are other interesting features seen in Fig. 4. First, note that variance spectra in the perturbed simulations are identical to those for unperturbed simulations over the first 12 to 24 h. As discussed previously,

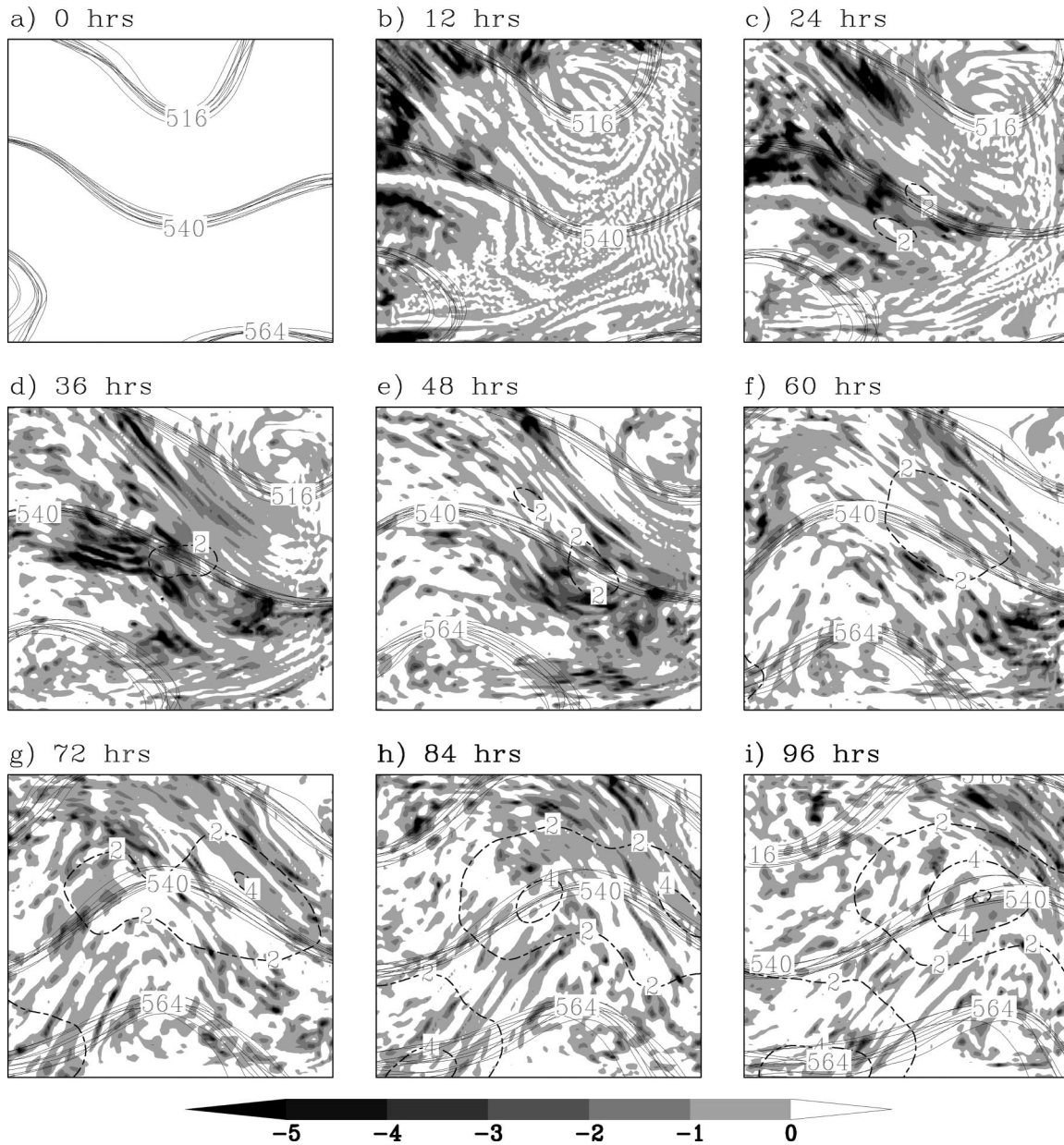


FIG. 3. Example case run on the medium domain with perturbations applied to 3-hourly updated, low-pass-filtered LBCs. A “spaghetti” plot drawn with solid black lines shows the $(516, 540, 564) \times 10^6 \text{ m}^2 \text{ s}^{-1}$ streamlines from each of the 10 LAM ensemble members. Reduction of vorticity dispersion is shaded, while streamfunction dispersion is shown with dashed contours at $2 \times 10^{12} \text{ m}^4 \text{ s}^{-2}$ intervals. Compare to Fig. 12 in Nutter et al. (2004).

the amplitude of the perturbation field is set to zero during this time because the LAM variance spectra exceed those of the global simulations. Note also that the error variance curves continue to oscillate because of the LBC error “pulse” caused by temporal interpolation between otherwise perfect LBCs (see Nutter et al. 2004).

LAM simulations were also conducted after adding perturbations to hourly and 6-hourly updated LBCs (not shown). Normalized error variances obtained from simulations having perturbed, hourly updated LBCs (not

shown) reveal that error variances from the perturbed LAM simulations are nearly superimposed with those from the laterally unbounded global ensemble simulations. This result shows that the LBC perturbations function as designed. However, the additional effort of applying LBC perturbations is not justified for hourly updated LBCs since error growth constraints are minimal for this configuration (Nutter 2003). Results from the LAM configuration having 6-hourly updated LBCs (not shown) reveal similar features as those in Fig. 4, al-

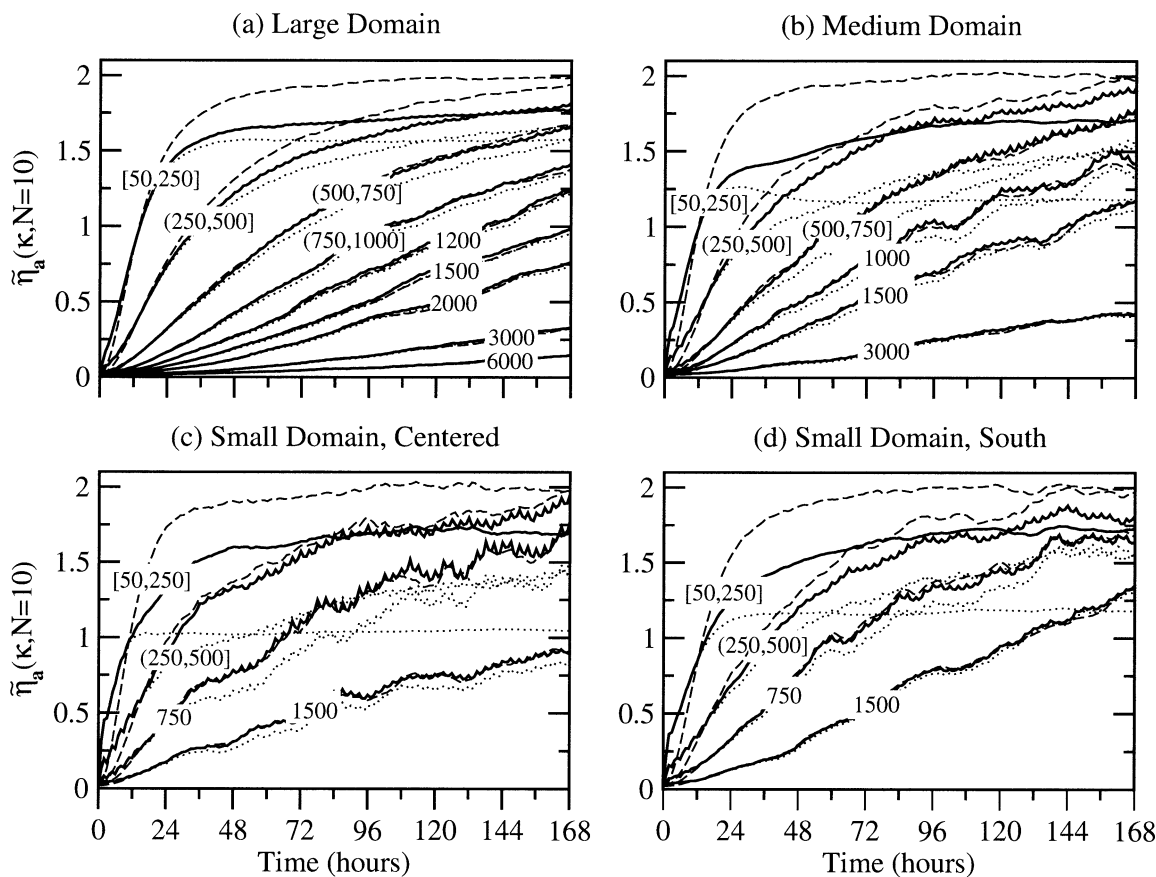


FIG. 4. Normalized vorticity error variance (solid lines), averaged over 100 independent 10-member LAM ensemble simulations having perturbed, 3-hourly updated, low-pass-filtered LBCs (150-km wavelength cutoff). Line labels (km) indicate wavelength(s) contributing to error variances. Dashed reference lines show error variances from subsets of global ensemble simulations, and dotted lines show error variances from corresponding LAM ensemble simulations run without LBC perturbations.

though the LBC perturbations are slightly less effective since they had a greater proportion of total variance to recover.

b. Ensemble summary statistics

It has been shown that the use of LBC perturbations capably restores much of the error variance lost by coarsely resolved and temporally interpolated external LBC fields, especially on smaller domains and at wavelengths longer than 250 km. *The primary goal of applying LBC perturbations is to restore LAM ensemble dispersion without adversely impacting the individual ensemble members.* Equation (1) provides a direct link between ensemble dispersion and the error variance evaluated in the previous subsection. It is useful to compare the relative magnitudes of each term in this equation to help determine what portion of total error variance (σ^2) contributes to ensemble dispersion (D^2) relative to the remaining bias terms. The ensemble mean square error (S^2) also is evaluated as an overall measure of performance.

Results are presented here for the model configuration

having perturbed, 3-hourly updated, low-pass-filtered (coarsely resolved) LBCs (Fig. 5). The loss of error variance at small scales due to LBC constraints was noted previously in Fig. 4. The integrated effect is a decrease in total error variance (σ^2) over the first 24–48 h of the simulation, depending on domain size. In previous simulations without LBC perturbations, the loss of total error variance leveled off at a near-constant value as LBC sweeping reached a balance with small-scale error growth on the interior of the LAM domain (see Nutter et al. 2004). In contrast, the amplitude of the LBC perturbations in the simulations shown here grow with time and begin to restore the total error variance. Consequently, the difference in spectra between global and LAM ensembles becomes less negative with time. The total error variance is not restored completely as noted in the previous section, but is most effectively restored on the smaller domains.

An interesting characteristic noted on all domains is the increase of total error variance in the LAM simulations during the first 12 h. Close examination of Fig. 4 shows that this increase in error variance is due to contributions at smaller scales. This extra variance ap-

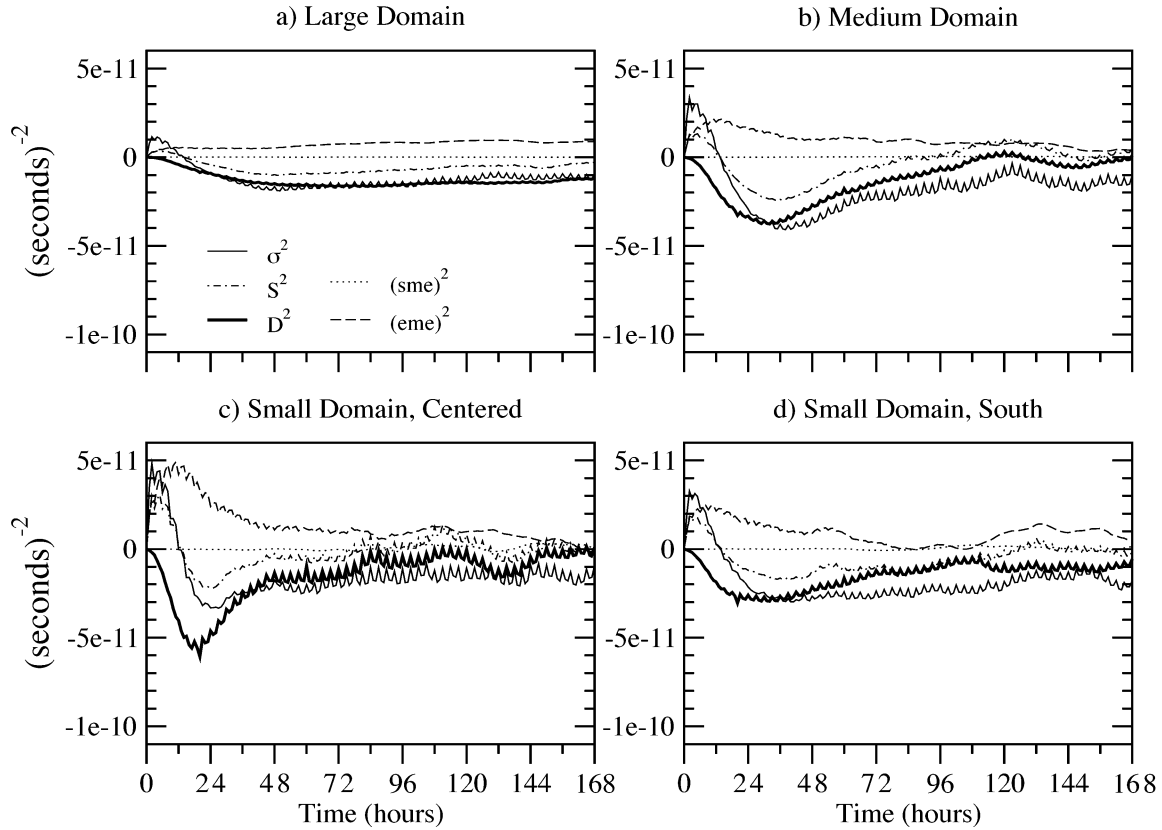


FIG. 5. Difference in vorticity summary statistics for LAM ensemble simulations having perturbed, 3-hourly updated, low-pass-filtered LBCs (150-km wavelength cutoff) compared to statistics from global ensemble simulations. Results are averaged over 100 independent 10-member ensemble simulations. Line labels in the legend are defined in section 2b. On ordinate, “e” denotes base-10 exponential notation.

pears early in the LAM simulations when the Helmholtz equation is inverted to obtain streamfunction from perturbed LBCs. In spite of the initial increase in error variance, LAM ensemble dispersion decreases for about 48 h in all simulations because of the increase in ensemble mean error in the absence of changes in the spatial bias [see Eq. (1)].

The ensemble statistics oscillate with time due to the LBC error pulse caused by temporal interpolation. The oscillation has a 3-h period associated with the interval at which LBCs are updated from external model fields. With each update, the external fields are perfect except for the removal of short waves by low-pass filtering to emulate coarse resolution and the subsequent addition of perturbations to restore variance at those scales.

The total error variance is fully restored when LBC perturbations are applied in LAM configurations having hourly updated LBCs (not shown). This result is expected since error variance spectra were restored at all wavelengths for this configuration (Nutter 2003). Furthermore, the use of LBC perturbations does not introduce additional spatial bias or ensemble mean error. Most importantly, when using hourly updated LBCs, LAM ensemble dispersion is fully restored to values obtained from corresponding subsets of global ensemble

simulations. Results from LAM configurations using 6-hourly simulations reveal similar results to those shown in Fig. 5.

5. Scaled LBC perturbations

Results shown in Fig. 4 reveal that the amplitude of LBC perturbations needed to fully restore error variance growth is underestimated under certain LAM configurations. Specifically, the perturbation amplitudes are underestimated at wavelengths shorter than 500 km, especially when applied to large domain simulations having coarsely resolved external LBCs updated at intervals of 3 h or longer. In an attempt to remedy this deficiency, the perturbation amplitudes were increased by applying a scale factor to the difference spectra $|F'(k, l)|^2$ [Eq. (10)]. The scale factor is defined as ratio of error variances obtained from perturbed LAM ensembles to those obtained from corresponding subdomains of global ensemble simulations. Thus, the difference spectra are redefined by introducing the scaling factor Λ so that

$$\Lambda = \sigma_{\kappa}^2(\text{global})/\sigma_{\kappa}^2(\text{perturbed LAM}) \quad \text{and} \quad (13)$$

$$|F'(k, l)|^2 = \Lambda[\sigma_{\kappa}^2(\text{global}) - \sigma_{\kappa}^2(\text{unperturbed LAM})]. \quad (14)$$

The use of scaled LBC perturbations did yield a small improvement for the LAM configuration having low-pass-filtered LBCs that were updated every 3 h (not shown). Given an increase in perturbation amplitudes of up to 40% after scaling, the increase in error variance at scales less than 500 km is about 0% to 6%. Although miniscule improvements were seen in the error variance spectra, the ensemble summary statistics (not shown) indicated that ensemble dispersion is almost unchanged compared to the configuration having unscaled LBC perturbations. Hence, the significance of these improvements using scaled LBC perturbations is questionable and not recommended given the additional computational expense.

6. Summary and discussion

A new method has been developed to apply LBC perturbations at every time step of LAM simulations. The LBC perturbations are intended to restore the small-scale error variances and ensemble dispersion lost due to coarsely resolved and temporally interpolated external LBC fields. Although the procedure outlined herein was developed within a simplified modeling system, the results suggest that LBC perturbation procedures can be implemented effectively to help relax the “one way” LBC constraints on LAM ensemble spread.

The LBC perturbation procedure is based on specifying a random field with desired spectral amplitudes and translating the field based on the Rossby wave dispersion relation. The advantage to this approach is that a coherent field is maintained through time while allowing for variable wave amplification and dispersion. It is a statistically based procedure, but is designed to mimic the dynamical behavior of the system. Simpler, purely statistical schemes such as an autoregressive, spatially correlated process cannot provide this desirable property.

Results showed that the application of LBC perturbations in LAM ensemble simulations capably restores error variances and ensemble dispersion to nearly the same values obtained from subsets of global ensemble simulations. Two exceptions were noted. First, error variances were not fully restored at wavelengths shorter than 500 km, especially for large domain simulations having coarsely resolved external LBC fields updated at intervals of 3 h or longer. This deficiency was attributed to the fact that short-wavelength LBC perturbations have small amplitudes and subsequently disperse and/or dissipate while propagating through the LAM domain. The second notable exception is that, in spite of the gain in error variance, ensemble dispersion for the small domains could not be fully recovered between about 12 and 48 h of the simulations. This deficiency was explained by the increase in ensemble mean error caused by coarsely resolved and temporally interpolated external LBC fields. The increase in ensemble mean error causes a decrease in ensemble dispersion that can-

not be recovered by the use of LBC perturbations as applied herein.

The LBC perturbations are based solely on differences in error variance spectra. Their only relationship to the dynamical evolution of flow inside the LAM domain is through the nonlinear advection term that transfers energy and enstrophy upscale and downscale throughout the spectrum. To ensure that the LBC perturbations do not overwhelm the quality of the LAM solution, it is necessary that their amplitudes remain small. Furthermore, the ensemble mean error can become inflated if the perturbations are too strong. An increase in ensemble mean error contributes to a loss of ensemble dispersion, which opposes the effort to restore dispersion through increases in error variance. Although not perfect in every aspect, the LBC perturbations developed in this work appear small enough to satisfy these concerns while restoring most of the ensemble dispersion and error variance lost through LBC constraints.

We conclude with comments on how this work may apply to more realistic modeling systems. Two fundamental assumptions were made at the start of this work (Nutter et al. 2004). First, it was assumed that natural error growth at large scales is (or can be) stated accurately using global model forecasts. This assumption is needed to ensure that error variances and ensemble dispersion are correct at wavelengths exceeding the breadth of the LAM domain. LBC perturbations are only effective at scales up to the size of the LAM domain and cannot correct deficiencies caused by improper error growth rates at larger scales. By design, the relative importance of LBC constraints on small-scale error variance has not been compared to those caused by deficiencies in large-scale error variances associated with the external model. To do so, one needs to account for different types of external model error originating through a variety of mechanisms. In practice, we must note that it is possible for large-scale variance constraints of external origin (e.g., Hacker and Baumhefner 2004) to overwhelm the effects of LBC constraints acting at small scales. A second assumption was made that error growth rates at small scales in LAMs should behave the same as those in global models operating at equivalent resolution. The amplitude of the LBC perturbations was determined by the difference in error variance spectra between global ensembles and LAM ensembles having unperturbed LBCs. So, again, the LBC perturbations may be less effective at restoring LAM ensemble spread if there are differences in the variance spectra caused by dynamical or artificial discrepancies between external and LAM models. A related assumption is that the model simulations are unbiased, since ensemble dispersion is linked to the total error variance, the ensemble mean error and the spatial bias. This secondary assumption is less important because corrections can be applied for systematic model errors. If corrections are not applied, then LBC perturbations

designed to restore error variance may not be as effective at directly restoring LAM ensemble dispersion.

A major obstacle faced in applying the LBC perturbation technique to other modeling systems is the determination of appropriate amplitude coefficients needed for constructing the perturbation fields. Global ensemble systems have been available for more than a decade. It should not be difficult to obtain error variance spectra over many cases for these ensembles, especially since most are integrated using spectral methods. The greater challenge is to obtain error variance spectra from LAM ensemble systems. LAM ensemble systems have existed for several years, but most do not include the statistical verification packages needed to calculate one-dimensional error variance spectra. Such packages would need to be developed, then results accumulated over many cases. Once an appropriate set of verification data has been accumulated, corrections for systematic errors must be applied before obtaining difference spectra. Finally, an issue that requires additional research is how to determine the vertical structure of LBC perturbations.

Temporal interpolation of coarsely resolved external LBC fields has been shown to remove small-scale features from LAM solutions and quickly sweep out any set of initial condition perturbations (Nutter et al. 2004). LBC perturbations applied at every time step will help offset the effects of these constraints on LAM ensemble spread. The perturbation procedure was developed for a simplified modeling system and does have notable limitations that can be enhanced when redeveloped for more practical applications. The effort will be most rewarding for independent organizations running LAMs on smaller domains where LBC sweeping effects act most quickly to constrain error growth rates. The additional expense of applying LBC perturbations may be offset by the ability to integrate LAM ensembles over smaller domains.

Acknowledgments. This research was supported by funding from several sources: the University of Oklahoma (OU) School of Meteorology through the Robert E. Lowry endowed chair; the U.S. Department of Defense under Grant N00014-96-1-1112, or Coastal Meteorology Research Program (CMRP); the Williams Energy Marketing and Trading Company through a Williams Graduate Research Fellowship within the OU Center for Analysis and Prediction of Storms (CAPS); the National Science Foundation under Grant ATM-0129892, related to the International H₂O Project (IHOP); and the OU Alumni Association Fellowship Program.

The National Severe Storms Laboratory (NSSL) shared desk space and access to a multiprocessor computer. The OU School of Meteorology provided excellent infrastructure and administrative support. Most of the computations were performed on the IBM Regatta p690 symmetric multiprocessor computer operated by

the OU Supercomputing Center for Education and Research (OSCAR).

Dr. Chris Snyder and a second anonymous reviewer provided useful comments that helped improve the manuscript.

REFERENCES

- Charney, J. G., R. Fjørtoft, and J. von Neumann, 1950: Numerical integration of the barotropic vorticity equation. *Tellus*, **2**, 237–254.
- Dalcher, A., and E. Kalnay, 1987: Error growth and predictability in operational ECMWF forecasts. *Tellus*, **39A**, 474–491.
- Davies, H. C., 1976: A lateral boundary formulation for multilevel prediction models. *Quart. J. Roy. Meteor. Soc.*, **102**, 405–418.
- , 1983: Limitations of some common lateral boundary schemes used in regional NWP models. *Mon. Wea. Rev.*, **111**, 1002–1012.
- De Elía, R., and R. Laprise, 2002: Forecasting skill limits of nested, limited-area models: A perfect-model approach. *Mon. Wea. Rev.*, **130**, 2006–2023.
- Errico, R. M., 1985: Spectra computed from a limited area grid. *Mon. Wea. Rev.*, **113**, 1554–1562.
- , and D. Baumhefner, 1987: Predictability experiments using a high-resolution limited-area model. *Mon. Wea. Rev.*, **115**, 488–504.
- Hacker, J. P., and D. P. Baumhefner, 2004: Flow-dependent calibration of ensemble spread using forecast spectra. Preprints, *16th Conf. on Numerical Weather Prediction*, Seattle, WA, Amer. Meteor. Soc., CD-ROM, 23.5.
- Hamill, T. M., 2001: Interpretation of rank histograms for verifying ensemble forecasts. *Mon. Wea. Rev.*, **129**, 550–560.
- , and S. J. Colucci, 1997: Verification of Eta-RSM short-range ensemble forecasts. *Mon. Wea. Rev.*, **125**, 1312–1327.
- Holton, J. R., 1979: *An Introduction to Dynamic Meteorology*. 2d ed. International Geophysics Series, Vol. 23, Academic Press, 391 pp.
- Hou, D., E. Kalnay, and K. K. Drogemeier, 2001: Objective verification of the SAMEX '98 ensemble forecasts. *Mon. Wea. Rev.*, **129**, 73–91.
- Laprise, R., M. R. Varma, B. Denis, D. Caya, and I. Zawadzki, 2000: Predictability of a nested limited-area model. *Mon. Wea. Rev.*, **128**, 4149–4154.
- Lorenz, E. N., 1982: Atmospheric predictability experiments with a large numerical model. *Tellus*, **34**, 505–513.
- Nutter, P., 2003: Effects of nesting frequency and lateral boundary perturbations on the dispersion of limited-area ensemble forecasts. Ph.D. dissertation, University of Oklahoma, 156 pp.
- , D. Stensrud, and M. Xue, 2004: Effects of coarsely resolved and temporally interpolated lateral boundary conditions on the dispersion of limited-area ensemble forecasts. *Mon. Wea. Rev.*, **132**, 2358–2377.
- Paegle, J., Q. Yang, and M. Wang, 1997: Predictability in limited area and global models. *Meteor. Atmos. Phys.*, **63**, 53–69.
- Press, W. H., S. A. Teukolsky, W. T. Vetterling, and B. P. Flannery, 1992: *Numerical Recipes in Fortran 77: The Art of Scientific Computing*. 2d ed. Cambridge University Press, 933 pp.
- Reynolds, C. A., P. J. Webster, and E. Kalnay, 1994: Random error growth in NMC's global forecasts. *Mon. Wea. Rev.*, **122**, 1281–1305.
- Schubert, S. D., and M. Suarez, 1989: Dynamical predictability in simple general circulation model: Average error growth. *J. Atmos. Sci.*, **46**, 353–370.
- Stroe, R., and J. F. Royer, 1993: Comparison of different error growth formulas and predictability estimation in numerical extended-range forecasts. *Ann. Geophys.*, **11**, 296–316.
- Vukicevic, T., and R. M. Errico, 1990: The influence of artificial and

- physical factors upon predictability estimates using a complex limited-area model. *Mon. Wea. Rev.*, **118**, 1460–1482.
- Walker, J. S., 1988: *Fourier Analysis*. Oxford University Press, 440 pp.
- Warner, T. T., R. A. Peterson, and R. E. Treadon, 1997: A tutorial on lateral boundary conditions as a basic and potentially serious limitation to regional numerical weather prediction. *Bull. Amer. Meteor. Soc.*, **78**, 2599–2617.